ACS APPLIED MATERIALS & INTERFACES

www.acsami.org

Research Article

Sequential Doping of Ladder-Type Conjugated Polymers for Thermally Stable n-Type Organic Conductors

Suhao Wang, Tero-Petri Ruoko, Gang Wang, Sergi Riera-Galindo, Sandra Hultmark, Yuttapoom Puttisong, Fabrizio Moro, Hongping Yan, Weimin M. Chen, Magnus Berggren, Christian Müller, and Simone Fabiano*

Cite This: *ACS Appl. Mater. Interfaces* 2020, 12, 53003−53011

Read Online

ACCESS | Metrics & More | Article Recommendations | Supporting Information

ABSTRACT: Doping of organic semiconductors is a powerful tool to optimize the performance of various organic (opto)electronic and bioelectronic devices. Despite recent advances, the low thermal stability of the electronic properties of doped polymers still represents a significant obstacle to implementing these materials into practical applications. Hence, the development of conducting doped polymers with excellent long-term stability at elevated temperatures is highly desirable. Here, we report on the sequential doping of the ladder-type polymer poly(benzimidazobenzophenanthroline) (BBL) with a benzimidazole-based dopant (i.e., N-DMBI). By combining electrical, UV−vis/infrared, X-ray diffraction, and electron paramagnetic resonance measurements, we quantitatively characterized the conductivity, Seebeck coefficient, spin density, and microstructure of the sequentially doped polymer films as a function of the thermal annealing temperature. Importantly, we observed that the electrical conductivity of N-DMBI-doped BBL remains unchanged even after 20 h of heating at 190 °C. This finding is remarkable and of particular interest for organic thermoelectrics.

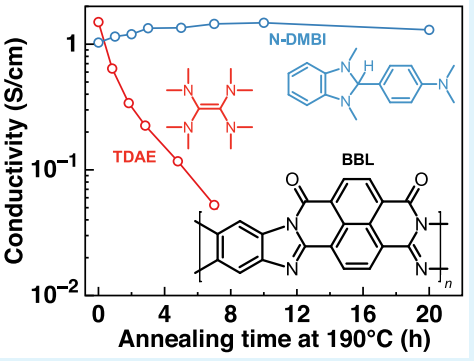

KEYWORDS: *conjugated polymers, sequential doping, n-doping, organic thermoelectrics, ladder-type polymers, thermal stability*

INTRODUCTION

Conjugated polymers have attracted a great deal of attention as a class of semiconducting materials that hold promise for the development of a wealth of traditional as well as unconventional low-cost and distributed technologies.[1−9] Their versatile chemical synthesis and inexpensive solution processability enable cost-efficient large-scale production of light, flexible, and even biocompatible electronic devices which would otherwise be difficult to realize using traditional inorganic semiconductors.[10−12] The electronic and electrical properties of π-conjugated polymers, and thus, the performance of the resulting (opto)electronic devices, depend strongly on the charge carrier concentration, which can be tuned by the so-called electrical doping.[13] Both p-doping and n-doping are needed to optimize various electronic devices, including organic solar cells, field-effect transistors, and thermoelectric generators.[14−22] This is typically achieved via an electron or proton/hydride transfer between the dopant molecule and the polymer backbone, a process that increases the charge carrier density and hence improves the electrical properties.[23] Conjugated polymers and molecular dopant molecules can either be coprocessed using a common solvent or sequentially processed by exposing the polymer film to the dopant vapors[24−26] or the dopant dissolved in an orthogonal solvent.[27,28] The advantage of sequential doping over coprocessing doping is that the morphology of the doped films remains to a large extent undisturbed,[28] thus yielding electrical conductivities that are superior to those commonly reached with coprocessing methods.[29]

Besides a high conductivity, the thermal stability of the electronic properties of doped polymers is a crucial parameter for many applications where high temperature operation is required, as in the case of solar cells and thermoelectrics. Although there exist many doped polymer systems that are stable upon mild thermal annealing, high temperature operation induces unfavorable diffusion and sublimation of the dopant molecules,[30] which eventually degrade the electrical properties and yield reduced device performance.[31−33] This is, for instance, the case of poly(3-hexylthiophene) (P3HT) p-doped with 2,3,5,6-tetrafluoro-7,7,8,8-tetracyanoquinodimethane (F_4TCNQ), which shows poor thermal stability above 90 °C because of the sublimation of F_4TCNQ.[34] Possible

Received: September 9, 2020
Accepted: October 29, 2020
Published: November 12, 2020

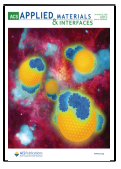

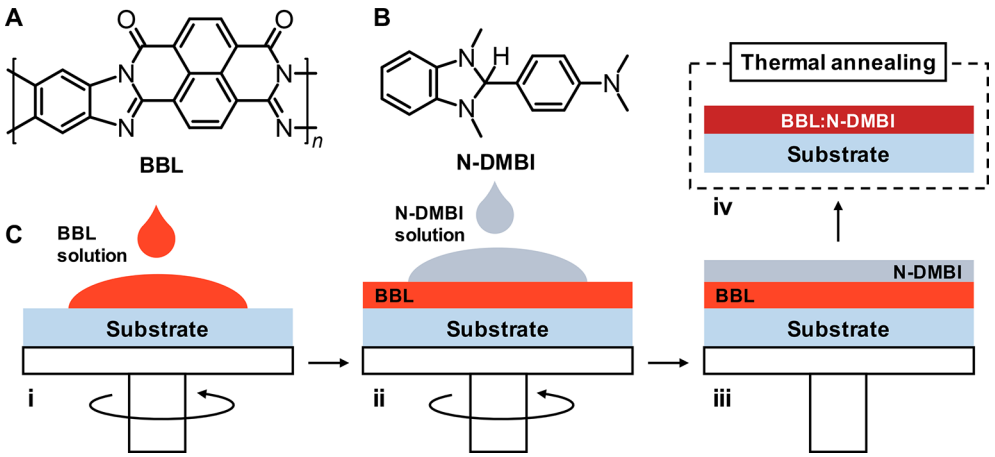

Figure 1. Chemical structures of (a) BBL and (b) N-DMBI. (c) Schematic illustration of the sequential doping process: (i) spin-coating of BBL; (ii) spin-coating of N-DMBI; (iii) resulting bilayer; and (iv) thermal annealing at different temperatures.

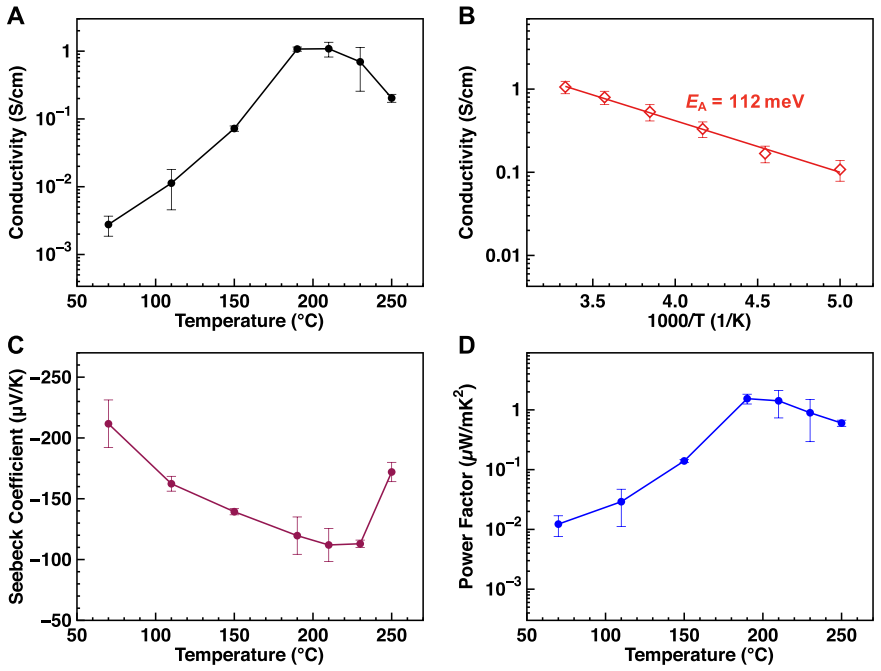

Figure 2. (a) Electrical conductivity of sequentially doped BBL as a function of thermal annealing temperature. (b) Temperature dependence of the electrical conductivity for the best doped BBL samples (annealed at 210 °C for 60 min). (c) Seebeck coefficient and (d) power factor of sequentially doped BBL films as a function of thermal annealing temperature.

strategies to improve the thermal stability of doped polymers are the use of conjugated polymeric dopants[35] or polyelectrolyte counterions[36] as well as the insertion of polar side chains in the polymer backbone to enhance the miscibility and compatibility of the dopant/polymer systems,[37,38] thus extending the operating temperature range.[39] However, the introduction of oligoethylene glycol side chains in the polymer backbone significantly lowers the polymer glass transition temperature, an effect which is known from solar cells to promote diffusivity of the acceptor molecule,[40] thus resulting in poor long-term stability. In this respect, the use of ladder-type conjugated polymers with a rigid and planar backbone might promote long-term stability at higher temperature. Poly(benzimidazobenzophenanthroline) (BBL) is the most notable example of electron-transporting ladder-type conducting polymers which shows an exceptionally high glass transition temperature (>500 °C).[41] BBL can be chemically[42] as well as electrochemically[43] doped to a high extent, thus reaching conductivity values that are larger than 1 S/cm. The high electrical conductivity derives from an extended charge carrier delocalization in the planar polymer backbone, which favors fast charge transport.[42] The main drawback is the limited solubility of BBL in common organic solvents that impede coprocessing with most of the typically used n-type dopants. For this reason, doping of BBL has most commonly been achieved by sequential processing via exposure to the volatile tetrakis(dimethylamino)ethylene (TDAE) dopant. However, because of the high surface pressure of TDAE and its reactivity with molecular oxygen,[44] the electrical properties of vapor-doped BBL films are typically not stable under ambient conditions and degrade quickly at elevated temperatures.[35]

Here, we report on the sequential doping of BBL with the air-stable benzimidazole derivative N-DMBI as a promising

https://dx.doi.org/10.1021/acsami.0c16254
ACS Appl. Mater. Interfaces 2020, 12, 53003−53011

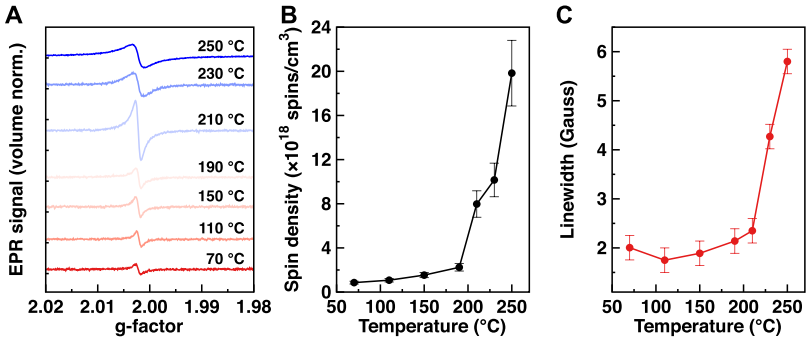

Figure 3. (a) EPR spectra (volume normalized), (b) spin density, and (c) linewidth of sequentially doped BBL films annealed at different temperatures.

method for the development of thermally stable n-type organic conductors. We observe that the doping level and thermoelectric properties of N-DMBI sequentially doped BBL films can be tuned by simply varying the thermal annealing temperature. Although the electrical conductivity of N-DMBI sequentially doped BBL is on par with that achieved with TDAE vapor doping (i.e., 1.1 ± 0.3 S cm^{-1}), N-DMBI sequentially doped BBL films exhibit far superior thermal and air stability as compared to the TDAE vapor-doped counterpart. Insights into the effect of processing conditions on the thermoelectric properties were gained through a combination of electrical measurements (electrical conductivity and Seebeck coefficient), electron paramagnetic resonance (EPR), UV−vis−NIR, and Fourier transform infrared (FTIR) spectroscopies, grazing incidence wide-angle X-ray scattering (GIWAXS), fast scanning calorimetry (FSC), and thermogravimetric analysis (TGA). Alongside achieving greatly improved stability with N-DMBI sequential doping when compared to TDAE vapor-doped BBL, we also attain a better understanding of the doping process and the polymer−dopant interactions in BBL.

RESULTS AND DISCUSSION

Electrical Measurements. Initially, we attempted to carry out doping of BBL by coprocessing with N-DMBI. Because BBL is only soluble in highly acidic solvents, N-DMBI and BBL were dissolved and blended in methanesulfonic acid (MSA). After spin-coating, the films were dipped into deionized water to remove residual MSA and then thermally annealed at 110 °C for 1 h. Very low conductivity values (<1 × 10^{-3} S cm^{-1}) were observed for all of the coprocessing doped BBL films, regardless of the N-DMBI-to-BBL monomer unit molar ratio (3−100%). Because N-DMBI is a weak base and the n-doping process progresses via either hydrogen removal or a thermally activated hydride transfer process,[45] we ascribe the low conductivity of the coprocessed films to inefficient doping with N-DMBI in the strongly acidic MSA solution.

Because of the marginal solubility of BBL in conventional organic solvents, sequential doping can be conveniently performed by choosing a suitable orthogonal solvent for the molecular dopant. Here, N-DMBI was dissolved in chloroform and spin-coated on top of the annealed dry BBL films, as schematically illustrated in Figure 1c. The films were then thermally annealed at different temperatures, as specified below. Figure 2a shows the evolution of the electrical conductivity of sequentially doped BBL films after thermal annealing for 60 min at temperatures ranging from 70 to 250 °C. When BBL films are thermally annealed at 70 °C, the conductivity is about 2.8 (±0.9) × 10^{-3} S cm^{-1} and dramatically increases up to 1.1 ± 0.3 S cm^{-1} for T = 210 °C. These values are comparable to those reported for TDAE vapor-doped and electrochemically reduced BBL films (1−2 S cm^{-1}),[42,46] suggesting a successful sequential doping process. Note also that the temperature range at which the conductivity reaches a maximum is compatible with most commercial, flexible plastic substrate materials such as polyether ether ketones, polyimides, and polyarylates.[47] At higher thermal annealing temperatures, the conductivity starts to decline, dropping to 0.7 ± 0.4 and 0.2 ± 0.03 S cm^{-1} for T = 230 and 250 °C, respectively (Figure 2a). We further compared the conductivities of samples annealed for different times (Figure S1a). The temperature-dependent conductivity has a similar trend for all annealing times (10, 60, and 180 min), except for temperatures starting at 210 °C, above which the longer annealing times result in a more pronounced loss of conductivity. We attribute this to the diffusion and evaporation of N-DMBI, which becomes more pronounced above 215 °C, as indicated by the mass loss observed by TGA (Figure S2). Variable-temperature conductivity measurements were performed on the N-DMBI sequentially doped BBL films annealed at 210 °C for 60 min, which yielded the highest conductivity (Figure 2b). The activation energy for charge transport was determined to be 112 ± 18 meV, which is comparable to the value previously reported for TDAE vapor-doped BBL (∼120 meV).[42]

We then measured the Seebeck coefficients (S) of the sequentially doped BBL films annealed at different temperatures in an inert environment. Figure 2c shows that S decreases monotonically upon increasing the thermal annealing temperatures from 70 to 210 °C, going from −212 ± 20 μV K^{-1} for T = 70 °C to −112 ± 14 μV K^{-1} for T = 210 °C. The negative sign of S agrees with the n-type nature of the sequentially doped films. The Seebeck coefficient of BBL films, annealed for different times, follows a similar but inverted trend as the conductivity, with longer annealing times at temperatures higher than 210 °C resulting in increased S (Figure S1b). Because the electrical conductivity and S are inversely interrelated, the power factor (PF = $S^2\sigma$) of sequentially doped BBL reaches a maximum at 1.5 ± 0.3 μW m^{-1} K^{-2} for an intermediate thermal annealing temperature of 190 °C (Figure 2d).

Thermal Analysis. TGA of N-DMBI indicates mass loss above 200 °C, with 5 wt % mass loss at 215 °C during heating at 10 °C min^{-1} (Figure S2a), which we assign to evaporation of the dopant. A differential scanning calorimetry (DSC) first heating thermogram of neat N-DMBI solidified by casting

https://dx.doi.org/10.1021/acsami.0c16254
ACS Appl. Mater. Interfaces 2020, 12, 53003−53011

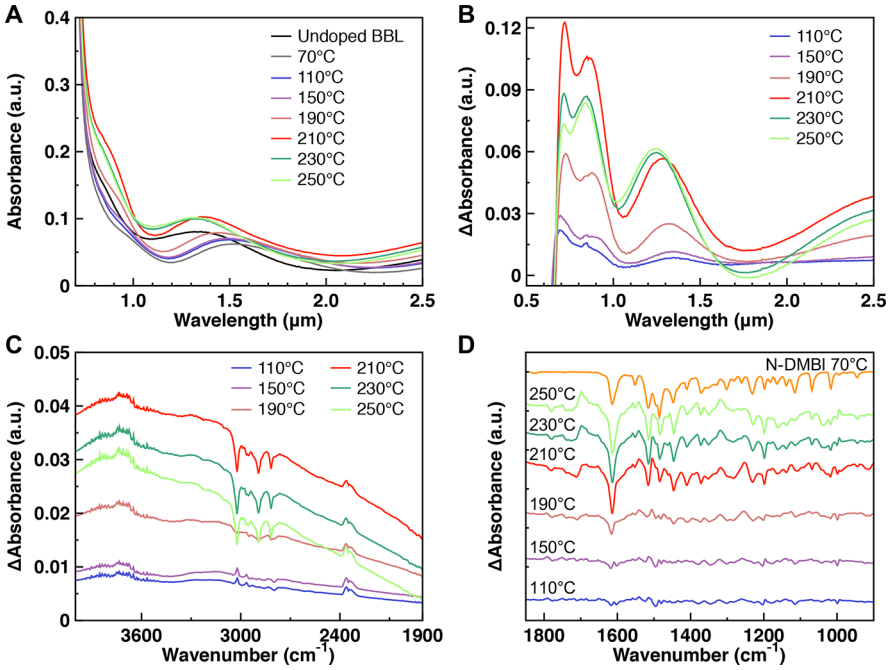

Figure 4. (a) UV−vis−NIR spectra, (b) differential UV−vis−NIR spectra, (c) differential FTIR spectra, and (d) stacked differential FTIR spectra of the same sequentially doped BBL film annealed progressively for 10 min at the indicated temperature. The differential spectra in b, c, and d are calculated by subtracting the spectrum of the sequentially doped BBL film annealed at 70 °C from the spectra measured after annealing at higher temperature. The spectrum labeled N-DMBI 70 °C in (d) is an inverted and scaled reference spectrum of an N-DMBI film annealed at 70 °C for reference.

from chloroform shows a distinct melting peak at T_m = 110 °C (Figure S2b). Cooling and second heating thermograms indicate that N-DMBI does not recrystallize but instead displays a distinct glass transition temperature T_g = −3 °C. We also carried out FSC to investigate the thermal behavior of N-DMBI/BBL bilayer films (see the Experimental Section for details). Repeated heating up to 195 °C results in flat and reproducible FSC thermograms (Figure S3), which indicates that no new thermal transitions arise because of contact of the dopant and polymer. Instead, heating up to 245 °C leads to a change in the slope of FSC thermograms, that is, a change in heat flow with temperature, which we explain with mass loss because of evaporation of the dopant (cf. Figure S3). Overall, our thermal analysis experiments allow us to rationalize the observed changes in conductivity upon annealing of N-DMBI/BBL films. We argue that annealing up to 200 °C leads to a strong increase in conductivity (cf. Figure 2a) because of diffusion of the dopant into the underlying BBL layer, which can readily take place above the T_m of N-DMBI. At temperatures above 210 °C, the dopant instead starts to evaporate, which correlates well with the optical and scattering analyses reported below (*vide infra*).

EPR Analysis. To shed light on the effect of thermal annealing on the charge density of sequentially doped BBL films, we performed EPR spectroscopy at room temperature. The samples were flame-sealed inside EPR quartz tubes filled with N_2. As shown in Figure 3a, an EPR signal arising from polarons was observed in the sequentially doped BBL film annealed at 70 °C. The extracted spin density continuously increases with increasing annealing temperature from 70 to 210 °C (Figure 3b), which agrees with the increases in conductivity observed over the same temperature range. Interestingly, however, unlike conductivity, the spin density continues to rise even at annealing temperatures above 210 °C. This further increase at T > 210 °C is accompanied by a surge in the EPR linewidth (Figure 3c), which we ascribed to an increase in energetic disorder induced by the decomposition of dopant molecules into radicals.[48] These immobile radicals could act as Coulomb scattering centers and negatively impact the charge carrier mobility, thus contributing, together with the evaporation of the dopant molecules, to the reduction in electrical conductivity observed in Figure 2a.

Optical Absorption Spectroscopy. We then used UV−vis−NIR absorption spectroscopy to investigate the optical absorption of pristine and sequentially doped BBL films on glass slides upon thermal annealing at different temperatures (Figure S4). The spectrum of pristine BBL features an intense absorption peak at ∼580 nm, assigned to the $\pi-\pi^*$ transition.[42] After sequential doping with N-DMBI, a broad absorption band centered around 800 nm appears, indicating the formation of negative polarons.[42] Compared to pristine BBL, the absorption of sequentially doped BBL is slightly blue-shifted. To study the optical changes arising from sequential doping of BBL in more detail, we deposited BBL on CaF_2 windows, which due to their wide transparency range enable transmission measurements with both UV−vis−NIR and FTIR spectroscopies of the same film. The UV−vis−NIR and differential UV−vis−NIR spectra in the range 500−2500 nm are presented in Figure 4, along with the differential FTIR spectra in the range 4000−900 cm^{-1} (see Figures S5 and S6 in the Supporting Information for the combined and raw FTIR spectra, respectively). The differential spectra were calculated by subtracting the spectrum of the N-DMBI/BBL film annealed at 70 °C from the spectra of the same film measured after annealing at higher temperatures.

Three wide polaronic absorption bands are visible for the sequentially doped BBL after annealing, located at 800, 1330, and 3600 nm (Figure S5). After the N-DMBI layer is deposited

https://dx.doi.org/10.1021/acsami.0c16254
ACS Appl. Mater. Interfaces 2020, 12, 53003−53011

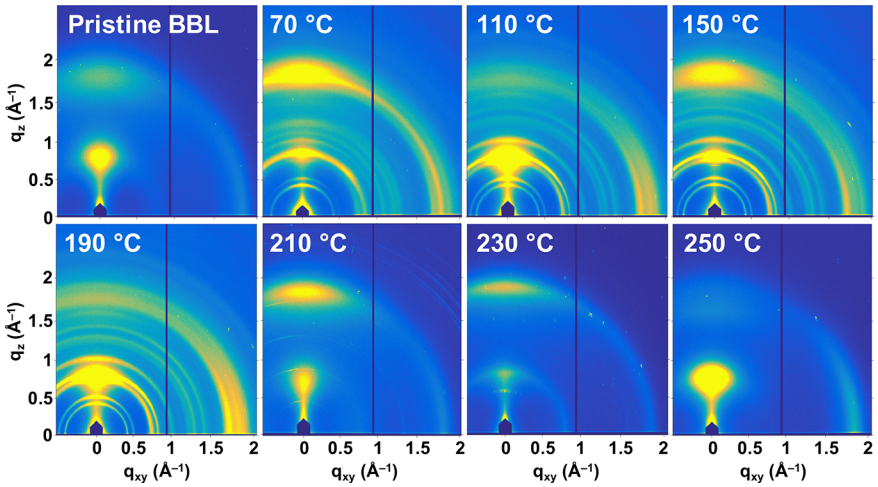

Figure 5. 2D-GIWAXS patterns of pristine and sequentially doped BBL thin films annealed at various temperatures.

on top of the BBL layer, the polaronic band located at 1330 nm experiences a red shift of ∼200 nm because of interference caused by the N-DMBI layer on top of the BBL film, gradually blue-shifting back to the original value after annealing at higher temperatures (see Table S1 in the Supporting Information for the peak wavelengths of this band at different annealing temperatures). The gradual blue-shift back to the value of pristine BBL is consistent with our argument that N-DMBI first gradually diffuses into the BBL film with the excess being expelled from the surface at the highest annealing temperatures (230 and 250 °C). Because of the red shift, we present the differential spectra for samples annealed at higher temperatures by subtracting the spectrum of sequentially doped BBL annealed at 70 °C in Figure 4. From the differential UV−vis−NIR spectra in Figure 4b, it can be seen that higher annealing temperatures increase the polaronic absorption bands until 210 °C, after which the polaronic absorption begins to decrease. This decrease coincides with the above discussed decomposition and evaporation of N-DMBI, and indicates that the doping level of BBL decreases at the highest annealing temperatures.

Vibrational Spectroscopy Characterization. The FTIR spectra in the range 4000−900 cm^{-1} are shown in Figure S6, with the corresponding differential FTIR spectra shown in Figure 4c,d. The spectra in Figures 4d and S6b are stacked for clarity. The FTIR spectrum of sequentially doped BBL is a superposition of the vibrational absorption bands of BBL and N-DMBI (see Table S2 in the Supporting Information for vibrational band assignment). In the differential spectra in Figure 4, only small changes are observed when the sample is annealed at 110 °C, which corresponds to the melting temperature of N-DMBI (Figure S2). Annealing the sample at 150 °C makes the changes more visible, with the formation of two new absorption bands between 1350 and 1250 cm^{-1} that we assign to polaronic absorption in BBL. At 190 °C, a shift in the BBL C═O vibration at 1700 cm^{-1} becomes visible, with the splitting of this band, forming a new absorption at 1650 cm^{-1} at higher annealing temperatures. We have previously shown that the C═O absorption splitting is the spectral fingerprint of polarons in the BBL structure.[49]

The annealing at 190 and 210 °C progressively decreases the N-DMBI absorption in the aromatic and methylamino C−H stretching absorptions around 3000 cm^{-1} and in the aromatic ring stretch between 1600 and 1500 cm^{-1} along with an increase in the polaronic absorption bands. No further loss of N-DMBI is observed after annealing at higher temperatures, suggesting that only N-DMBI that has reacted with BBL remains in the film. In order to track the amount of N-DMBI in sequentially doped BBL, we integrated the N-DMBI peaks in the C−H vibration and aromatic ring stretching regions after annealing at various temperatures (Figure S7). This shows that the amount of N-DMBI decreases drastically after annealing at 190 °C, with only a small amount (∼10%) remaining after annealing the film at 210 °C because of the evaporation of N-DMBI on top of the BBL film. This is in line with the observed decreases in conductivity and matches also with the observed weight loss in the TGA measurements of N-DMBI (Figure S2). Furthermore, we see a progressive decrease in the polaronic absorption band at 1250 cm^{-1}. This is a clear indication that sequential doping of BBL with N-DMBI works progressively when annealed until 210 °C, after which we observe a loss in N-DMBI content. Note that both UV−vis−NIR and FTIR measurements indicate a reduction in the polaron concentration for T > 210 °C, suggesting that the radicals contributing to the EPR signal (cf. Figure 3) do not sit on BBL chains.

Film Microstructure and Molecular Packing. GIWAXS was performed to investigate the microstructure evolution of sequentially doped BBL films annealed at various temperatures. The 2D-GIWAXS diffraction images are shown in Figure 5, with the corresponding line-cut plots in Figure S8 and the variation of the (100) and (010) d-spacings of the pristine and doped BBL films in Figure S9. Undoped BBL has a preferential edge-on orientation with a lamellar (100) peak in the q_z plane at 0.79 $Å^{-1}$ (d-spacing = 7.92 Å) and an in-plane $\pi-\pi$ stacking (010) peak at q_{xy} = 1.83 $Å^{-1}$ (d-spacing = 3.43 Å). This is in good agreement with the previously reported diffraction pattern of undoped BBL thin films.[35,50] Sequential doping decreases the out-of-plane lamellar stacking of BBL (Figure S9a), whereas the $\pi-\pi$ stacking is slightly increased (Figures S9b). Several peaks that are attributed to the diffraction of N-DMBI aggregates (Figure S10) are also visible for the samples annealed between 70 and 190 °C (Figure 5). When annealed at 210 °C, the N-DMBI peaks largely disappear, corresponding well with the FTIR data indicating a sharp decrease in the amount of N-DMBI because of evaporation, along with a sharp increase in the intrachain stacking and gradual decrease in the interchain stacking. This

https://dx.doi.org/10.1021/acsami.0c16254
ACS Appl. Mater. Interfaces 2020, 12, 53003−53011

suggests that N-DMBI is removed from the sequentially doped BBL films when annealed at $T \geq 210$ °C.

Electrical Stability Measurements. Finally, we tested the thermal and ambient stability of BBL sequentially doped with N-DMBI and compared it to that of TDAE vapor-doped BBL. As shown in Figure 6a, the electrical conductivity of TDAE

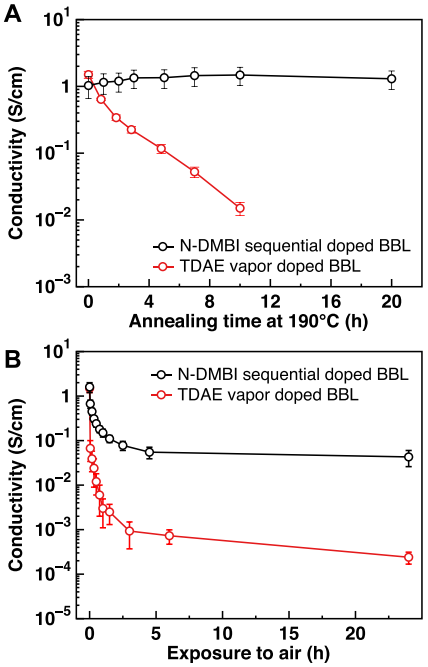

Figure 6. Electrical stability test of TDAE vapor-doped and N-DMBI sequentially doped BBL films (a) annealed at 190 °C for 20 h in N_2 and (b) exposed to air.

vapor-doped BBL films dropped by 2 orders of magnitude upon heating the samples at 190 °C for 10 h. In contrast, the electrical conductivity of N-DMBI sequentially doped BBL remained unchanged even after 20 h of heating, revealing the remarkable thermal stability of these films. Furthermore, although both N-DMBI sequentially doped BBL and TDAE vapor-doped BBL films are stable in a N_2 atmosphere, the former exhibits significantly higher stability in air, which we attributed to the higher ambient stability of N-DMBI as compared to TDAE. As shown in Figure 6b, after exposing the films to ambient conditions for 5 h, N-DMBI sequentially doped BBL shows conductivities 2 orders of magnitude higher than TDAE vapor-doped BBL. The conductivity of N-DMBI sequentially doped BBL did not decrease further after 24 h of exposure. Although N-DMBI is a relatively air-stable n-type dopant,[51] TDAE is inherently unstable in ambient and undergoes chemiluminescence in the presence of oxygen.[44] We believe that this is at the origin of the improved ambient stability of N-DMBI-doped BBL. Our results show conclusively that N-DMBI sequentially doped BBL is more stable than TDAE vapor-doped BBL under ambient conditions and especially at high temperatures, even though the conductivities of both were similar before exposure.

CONCLUSIONS

In conclusion, we show that N-DMBI sequential doping of BBL is an effective way to obtain highly conductive films while achieving ambient and thermal stability far superior to those of state-of-the-art TDAE vapor-doped BBL. Sequential doping with N-DMBI is thermally activated, and the doping level can be reproducibly tuned by simply changing the annealing temperature. Optical spectroscopy measurements show that the polaron concentration in the doped films follows the same trend as the conductivity, and the doping level increases until the evaporation temperature of N-DMBI is reached. Our work offers feasible guidelines for developing efficient n-type organic electronic devices with improved stability.

EXPERIMENTAL SECTION

Thin-Film Preparation and Sequential Doping. All thin films were deposited on top of glass substrates, which were cleaned by sonicating in water, acetone, and isopropanol, for 10 min each, followed by drying with nitrogen. BBL (purchased from Sigma-Aldrich) was dissolved in methanesulfonic acid (MSA) at a concentration of 7.5 mg/mL. To ensure full dissolution of BBL, the solution was stirred at 70 °C for 2 h. The warm solution (70 °C) was deposited onto the glass substrates by spin-coating at 500 rpm for 30 s. Immediately after spin-coating, the BBL films were dipped into deionized water to remove residual MSA. The obtained BBL films were dried first in an oven at 100 °C to remove the water and then thermally annealed on a hot plate at 200 °C in a glovebox filled with nitrogen for 1 h, yielding films with a thickness of 40 nm. To sequentially dope the BBL films, solutions of N-DMBI (purchased from Sigma-Aldrich) were first dissolved in $CHCL_3$ at 10 mg/mL and deposited on top of pristine BBL thin films by spin-coating at 1500 rpm. To tune the doping levels, the sequentially doped BBL films were annealed on a hot plate at various temperatures ranging from 70 to 250 °C inside the glovebox.

Electrical Characterization. Electrical conductivity and Seebeck coefficient were measured inside a nitrogen-filled glovebox using a Keithley 4200-SCS. For measurements reported in Figures 2a,c,d and S1b, Au electrodes with a Ti adhesion layer (Au/Ti = 25 nm/5 nm, L/W = 0.5 mm/15 mm) were deposited on top of glass substrates prior to polymer layer deposition. For conductivity measurements in Figures 2b and S1a, we fabricated electrodes with a shorter channel length (L/W = 30 μm/1000 μm). The temperature gradient (ΔT) across the sample was applied with two Peltier modules, and the thermovoltage (ΔV) was measured between two separate electrodes (L/W = 0.5 mm/15 mm). The S was calculated from the slope of ΔV measured at six different ΔT values. It is worth to mention that we used an electrode configuration (aspect ratio of the electrodes We/Le = 30) which takes the effect of the contact geometry into consideration.[52] This configuration enables minimizing the error in determining S, resulting in smaller sample-to-sample variation.

Spectroscopy Characterization. Optical UV−vis−NIR spectra of pristine BBL and sequentially doped BBL films were measured under a nitrogen atmosphere at room temperature with PerkinElmer Lambda 900. FTIR spectra in the mid-IR region were measured inside an air-tight sample holder with a N_2-purged Bruker Equinox 55 FTIR spectrometer in the transmission mode between 4000 and 900 cm^{-1} with a resolution of 4 cm^{-1} and a zero-filling factor of 2 using 200 scan averaging.

Quantitative EPR experiments were carried out at the Swedish Interdisciplinary Magnetic Resonance Centre (SIMARC) at Linköping University, using a Bruker Elexsys E500 spectrometer operating at 9.8 GHz (X-band). All spectra were recorded in the dark at room temperature. Quantitative spin counting was calibrated with a standard sample. All EPR spectra were normalized using an effective detection volume of the samples.

Thermal Analysis. TGA was carried out under nitrogen flow between 25 and 500 °C with a scan rate of 10 °C/min using a Mettler Toledo TGA/DSC 3 + instrument. Differential scanning calorimetry (DSC) measurements were carried out under nitrogen flow between −50 and 150 °C with a scan rate of 10 °C/min using a Mettler Toledo DSC2 calorimeter. The sample weight for both TGA and DSC was 4 mg. FSC was carried out under nitrogen flow between

https://dx.doi.org/10.1021/acsami.0c16254
ACS Appl. Mater. Interfaces 2020, 12, 53003−53011

−30 and 195 or 245 °C at a scan rate of 4000 °C/s using a Mettler Toledo Flash DSC 1 instrument. Samples for FSC were prepared by spin-coating the BBL thin film on top of a layer of polymethyl methacrylate (PMMA) and dissolving the PMMA in acetone to release the BBL film. The BBL thin film was deposited on a Mettler Toledo MultiSTAR UFS1 sensor, followed by sequential doping through spin-coating with a solution of N-DMBI with a concentration of 10 mg/mL in $CHCl_3$.

Grazing Incidence Wide-Angle X-ray Scattering. GIWAXS was measured at Argonne National Laboratory at Beamline 8-ID-E at the advanced photon source (APS). The substrate surface was aligned at an incident angle of 0.130−0.140° with regard to the incoming X-ray beam. The samples were irradiated with a 10.915 keV X-ray beam in air for 2 summed exposures of 3 s (altogether 6 s). The scattered beam was recorded with a Pilatus 1 M detector located 228.165 mm away from the sample. Finally, the captured images were processed by employing the GIXGUI software. The background was subtracted by fitting the curves to an exponential decay, and the peaks were fitted to Gaussian functions.

■ ASSOCIATED CONTENT

Supporting Information

The Supporting Information is available free of charge at https://pubs.acs.org/doi/10.1021/acsami.0c16254.

Additional characterization data, such as DSC, TGA, UV−vis−NIR−MIR, FTIR, and GIWAXS and FSC investigation (PDF)

■ AUTHOR INFORMATION

Corresponding Author

Simone Fabiano − *Laboratory of Organic Electronics, Department of Science and Technology, Linköping University, 60174 Norrköping, Sweden;* orcid.org/0000-0001-7016-6514; Email: simone.fabiano@liu.se

Authors

Suhao Wang − *Laboratory of Organic Electronics, Department of Science and Technology, Linköping University, 60174 Norrköping, Sweden;* orcid.org/0000-0002-6295-7639

Tero-Petri Ruoko − *Laboratory of Organic Electronics, Department of Science and Technology, Linköping University, 60174 Norrköping, Sweden;* orcid.org/0000-0003-3091-1051

Gang Wang − *Laboratory of Organic Electronics, Department of Science and Technology, Linköping University, 60174 Norrköping, Sweden*

Sergi Riera-Galindo − *Laboratory of Organic Electronics, Department of Science and Technology, Linköping University, 60174 Norrköping, Sweden;* orcid.org/0000-0003-4221-0367

Sandra Hultmark − *Department of Chemistry and Chemical Engineering, Chalmers University of Technology, 41296 Goteborg, Sweden*

Yuttapoom Puttisong − *Department of Physics, Chemistry and Biology, Linköping University, 58183 Linköping, Sweden;* orcid.org/0000-0002-9690-6231

Fabrizio Moro − *Department of Physics, Chemistry and Biology, Linköping University, 58183 Linköping, Sweden*

Hongping Yan − *Stanford Synchrotron Radiation Light Source, SLAC National Accelerator Laboratory, Menlo Park 94025, California, United States;* orcid.org/0000-0001-6235-4523

Weimin M. Chen − *Department of Physics, Chemistry and Biology, Linköping University, 58183 Linköping, Sweden;* orcid.org/0000-0002-6405-9509

Magnus Berggren − *Laboratory of Organic Electronics, Department of Science and Technology, Linköping University, 60174 Norrköping, Sweden*

Christian Müller − *Department of Chemistry and Chemical Engineering, Chalmers University of Technology, 41296 Goteborg, Sweden;* orcid.org/0000-0001-7859-7909

Complete contact information is available at: https://pubs.acs.org/10.1021/acsami.0c16254

Author Contributions

S.W. and T.-P.R. contributed equally. The manuscript was written through contributions of all authors. All authors have given approval to the final version of the manuscript.

Notes

The authors declare no competing financial interest.

■ ACKNOWLEDGMENTS

The authors thank Sepideh Zokaei (Chalmers) for help with TGA measurements. S.F. acknowledges the support from the Swedish Research Council (2016-03979), ÅForsk (18-313, 19-310), and Olle Engkvists Stiftelse (204-0256). S.F. and W.M.C. acknowledge financial support from the Swedish Government Strategic Research Area in Materials Science on Functional Materials at Linköping University (Faculty Grant SFO-Mat-LiU No 2009 00971). T.-P.R. acknowledges financial support from the Finnish Cultural Foundation and the Finnish Foundation for Technology Promotion. S.H. and C.M. acknowledge financial support from the Knut and Alice Wallenberg Foundation through the project "Mastering Morphology for Solution-borne Electronics". W.M.C. acknowledges financial support from the Knut and Alice Wallenberg Foundation (Dnr KAW 2014.0041).

■ REFERENCES

(1) Facchetti, A. Semiconductors for organic transistors. *Mater. Today* **2007**, *10*, 28−37.

(2) Xu, J.; Wang, S.; Wang, G.-J. N.; Zhu, C.; Luo, S.; Jin, L.; Gu, X.; Chen, S.; Feig, V. R.; To, J. W. F.; Rondeau-Gagné, S.; Park, J.; Schroeder, B. C.; Lu, C.; Oh, J. Y.; Wang, Y.; Kim, Y.-H.; Yan, H.; Sinclair, R.; Zhou, D.; Xue, G.; Murmann, B.; Linder, C.; Cai, W.; Tok, J. B.-H.; Chung, J. W.; Bao, Z. Highly stretchable polymer semiconductor films through the nanoconfinement effect. *Science* **2017**, *355*, 59−64.

(3) Sekitani, T.; Someya, T. Stretchable, Large-area Organic Electronics. *Adv. Mater.* **2010**, *22*, 2228−2246.

(4) Bucella, S. G.; Luzio, A.; Gann, E.; Thomsen, L.; McNeill, C. R.; Pace, G.; Perinot, A.; Chen, Z.; Facchetti, A.; Caironi, M. Macroscopic and high-throughput printing of aligned nanostructured polymer semiconductors for MHz large-area electronics. *Nat. Commun.* **2015**, *6*, 8394.

(5) Suarez, F.; Nozariasbmarz, A.; Vashaee, D.; Öztürk, M. C. Designing thermoelectric generators for self-powered wearable electronics. *Energy Environ. Sci.* **2016**, *9*, 2099−2113.

(6) Rivnay, J.; Inal, S.; Salleo, A.; Owens, R. M.; Berggren, M.; Malliaras, G. G. Organic electrochemical transistors. *Nat. Rev. Mater.* **2018**, *3*, 17086.

(7) Ohayon, D.; Nikiforidis, G.; Savva, A.; Giugni, A.; Wustoni, S.; Palanisamy, T.; Chen, X.; Maria, I. P.; Di Fabrizio, E.; Costa, P. M. F. J.; McCulloch, I.; Inal, S. Biofuel powered glucose detection in bodily fluids with an n-type conjugated polymer. *Nat. Mater.* **2020**, *19*, 456−463.

(8) Andersson Ersman, P.; Lassnig, R.; Strandberg, J.; Tu, D.; Keshmiri, V.; Forchheimer, R.; Fabiano, S.; Gustafsson, G.; Berggren, M. All-printed large-scale integrated circuits based on organic electrochemical transistors. *Nat. Commun.* **2019**, *10*, 5053.
(9) Fuller, E. J.; Keene, S. T.; Melianas, A.; Wang, Z.; Agarwal, S.; Li, Y.; Tuchman, Y.; James, C. D.; Marinella, M. J.; Yang, J. J.; Salleo, A.; Talin, A. A. Parallel programming of an ionic floating-gate memory array for scalable neuromorphic computing. *Science* **2019**, *364*, 570−574.
(10) Facchetti, A. π-Conjugated Polymers for Organic Electronics and Photovoltaic Cell Applications†. *Chem. Mater.* **2011**, *23*, 733−758.
(11) Root, S. E.; Savagatrup, S.; Printz, A. D.; Rodriquez, D.; Lipomi, D. J. Mechanical Properties of Organic Semiconductors for Stretchable, Highly Flexible, and Mechanically Robust Electronics. *Chem. Rev.* **2017**, *117*, 6467−6499.
(12) Pappa, A. M.; Ohayon, D.; Giovannitti, A.; Maria, I. P.; Savva, A.; Uguz, I.; Rivnay, J.; McCulloch, I.; Owens, R. M.; Inal, S. Direct metabolite detection with an n-type accumulation mode organic electrochemical transistor. *Sci. Adv.* **2018**, *4*, No. eaat0911.
(13) Salzmann, I.; Heimel, G.; Oehzelt, M.; Winkler, S.; Koch, N. Molecular Electrical Doping of Organic Semiconductors: Fundamental Mechanisms and Emerging Dopant Design Rules. *Acc. Chem. Res.* **2016**, *49*, 370−378.
(14) Zhang, Y.; Zhou, H.; Seifter, J.; Ying, L.; Mikhailovsky, A.; Heeger, A. J.; Bazan, G. C.; Nguyen, T.-Q. Molecular Doping Enhances Photoconductivity in Polymer Bulk Heterojunction Solar Cells. *Adv. Mater.* **2013**, *25*, 7038−7044.
(15) Zhou, Y.; Fuentes-Hernandez, C.; Shim, J.; Meyer, J.; Giordano, A. J.; Li, H.; Winget, P.; Papadopoulos, T.; Cheun, H.; Kim, J.; Fenoll, M.; Dindar, A.; Haske, W.; Najafabadi, E.; Khan, T. M.; Sojoudi, H.; Barlow, S.; Graham, S.; Bredas, J.-L.; Marder, S. R.; Kahn, A.; Kippelen, B. A Universal Method to Produce Low-Work Function Electrodes for Organic Electronics. *Science* **2012**, *336*, 327−332.
(16) Kroon, R.; Mengistie, D. A.; Kiefer, D.; Hynynen, J.; Ryan, J. D.; Yu, L.; Müller, C. Thermoelectric plastics: from design to synthesis, processing and structure-property relationships. *Chem. Soc. Rev.* **2016**, *45*, 6147−6164.
(17) Lu, G.; Blakesley, J.; Himmelberger, S.; Pingel, P.; Frisch, J.; Lieberwirth, I.; Salzmann, I.; Oehzelt, M.; Di Pietro, R.; Salleo, A.; Koch, N.; Neher, D. Moderate doping leads to high performance of semiconductor/insulator polymer blend transistors. *Nat. Commun.* **2013**, *4*, 1588.
(18) Lüssem, B.; Keum, C.-M.; Kasemann, D.; Naab, B.; Bao, Z.; Leo, K. Doped Organic Transistors. *Chem. Rev.* **2016**, *116*, 13714−13751.
(19) Glaudell, A. M.; Cochran, J. E.; Patel, S. N.; Chabinyc, M. L. Impact of the Doping Method on Conductivity and Thermopower in Semiconducting Polythiophenes. *Adv. Energy Mater.* **2015**, *5*, 1401072.
(20) Wolfe, R. M. W.; Menon, A. K.; Marder, S. R.; Reynolds, J. R.; Yee, S. K. Thermoelectric Performance of n-Type Poly(Ni-tetrathiooxalate) as a Counterpart to Poly(Ni-ethenetetrathiolate): NiTTO versus NiETT. *Adv. Electron. Mater.* **2019**, *5*, 1900066.
(21) Ueda, K.; Yamada, Y.; Terao, T.; Manabe, K.; Hirai, T.; Asaumi, Y.; Fujii, S.; Kawano, S.; Muraoka, M.; Murata, M. High-performance, air-stable, n-type thermoelectric films from a water-dispersed nickel-ethenetetrathiolate complex and ethylene glycol. *J. Mater. Chem. A* **2020**, *8*, 12319−12322.
(22) Liu, J.; Garman, M. P.; Dong, J.; van der Zee, B.; Qiu, L.; Portale, G.; Hummelen, J. C.; Koster, L. J. A. Doping Engineering Enables Highly Conductive and Thermally Stable n-Type Organic Thermoelectrics with High Power Factor. *ACS Appl. Energy Mater.* **2019**, *2*, 6664−6671.
(23) Riera-Galindo, S.; Orbelli Biroli, A.; Forni, A.; Puttisong, Y.; Tessore, F.; Pizzotti, M.; Pavlopoulou, E.; Solano, E.; Wang, S.; Wang, G.; Ruoko, T.-P.; Chen, W. M.; Kemerink, M.; Berggren, M.; di Carlo, G.; Fabiano, S. Impact of Singly Occupied Molecular Orbital Energy on the n-Doping Efficiency of Benzimidazole Derivatives. *ACS Appl. Mater. Interfaces* **2019**, *11*, 37981−37990.
(24) Kang, K.; Watanabe, S.; Broch, K.; Sepe, A.; Brown, A.; Nasrallah, I.; Nikolka, M.; Fei, Z.; Heeney, M.; Matsumoto, D.; Marumoto, K.; Tanaka, H.; Kuroda, S.-i.; Sirringhaus, H. 2D coherent charge transport in highly ordered conducting polymers doped by solid state diffusion. *Nat. Mater.* **2016**, *15*, 896.
(25) Patel, S. N.; Glaudell, A. M.; Peterson, K. A.; Thomas, E. M.; O'Hara, K. A.; Lim, E.; Chabinyc, M. L. Morphology controls the thermoelectric power factor of a doped semiconducting polymer. *Sci. Adv.* **2017**, *3*, No. e1700434.
(26) Wang, S.; Sun, H.; Erdmann, T.; Wang, G.; Fazzi, D.; Lappan, U.; Puttisong, Y.; Chen, Z.; Berggren, M.; Crispin, X.; Kiriy, A.; Voit, B.; Marks, T. J.; Fabiano, S.; Facchetti, A. A Chemically Doped Naphthalenediimide-Bithiazole Polymer for n-Type Organic Thermoelectrics. *Adv. Mater.* **2018**, *30*, 1801898.
(27) Chew, A. R.; Ghosh, R.; Shang, Z.; Spano, F. C.; Salleo, A. Sequential Doping Reveals the Importance of Amorphous Chain Rigidity in Charge Transport of Semi-Crystalline Polymers. *J. Phys. Chem. Lett.* **2017**, *8*, 4974−4980.
(28) Jacobs, I. E.; Aasen, E. W.; Oliveira, J. L.; Fonseca, T. N.; Roehling, J. D.; Li, J.; Zhang, G.; Augustine, M. P.; Mascal, M.; Moulé, A. J. Comparison of solution-mixed and sequentially processed P3HT:F4TCNQ films: effect of doping-induced aggregation on film morphology. *J. Mater. Chem. C* **2016**, *4*, 3454−3466.
(29) Nava, D.; Shin, Y.; Massetti, M.; Jiao, X.; Biskup, T.; Jagadeesh, M. S.; Calloni, A.; Duò, L.; Lanzani, G.; McNeill, C. R.; Sommer, M.; Caironi, M. Drastic Improvement of Air Stability in an n-Type Doped Naphthalene-Diimide Polymer by Thionation. *ACS Appl. Energy Mater.* **2018**, *1*, 4626−4634.
(30) Li, J.; Koshnick, C.; Diallo, S. O.; Ackling, S.; Huang, D. M.; Jacobs, I. E.; Harrelson, T. F.; Hong, K.; Zhang, G.; Beckett, J.; Mascal, M.; Moulé, A. J. Quantitative Measurements of the Temperature-Dependent Microscopic and Macroscopic Dynamics of a Molecular Dopant in a Conjugated Polymer. *Macromolecules* **2017**, *50*, 5476−5489.
(31) Li, J.; Rochester, C. W.; Jacobs, I. E.; Friedrich, S.; Stroeve, P.; Riede, M.; Moulé, A. J. Measurement of Small Molecular Dopant F4TCNQ and C60F36 Diffusion in Organic Bilayer Architectures. *ACS Appl. Mater. Interfaces* **2015**, *7*, 28420−28428.
(32) Jacobs, I. E.; Moulé, A. J. Controlling Molecular Doping in Organic Semiconductors. *Adv. Mater.* **2017**, *29*, 1703063.
(33) Kroon, R.; Kiefer, D.; Stegerer, D.; Yu, L.; Sommer, M.; Müller, C. Polar Side Chains Enhance Processability, Electrical Conductivity, and Thermal Stability of a Molecularly p-Doped Polythiophene. *Adv. Mater.* **2017**, *29*, 1700930.
(34) Li, J.; Rochester, C. W.; Jacobs, I. E.; Aasen, E. W.; Friedrich, S.; Stroeve, P.; Moulé, A. J. The effect of thermal annealing on dopant site choice in conjugated polymers. *Org. Electron.* **2016**, *33*, 23−31.
(35) Xu, K.; Sun, H.; Ruoko, T.-P.; Wang, G.; Kroon, R.; Kolhe, N. B.; Puttisong, Y.; Liu, X.; Fazzi, D.; Shibata, K.; Yang, C.-Y.; Sun, N.; Persson, G.; Yankovich, A. B.; Olsson, E.; Yoshida, H.; Chen, W. M.; Fahlman, M.; Kemerink, M.; Jenekhe, S. A.; Müller, C.; Berggren, M.; Fabiano, S. Ground-state electron transfer in all-polymer donor-acceptor heterojunctions. *Nat. Mater.* **2020**, *19*, 738−744.
(36) Kim, S.-M.; Kim, C.-H.; Kim, Y.; Kim, N.; Lee, W.-J.; Lee, E.-H.; Kim, D.; Park, S.; Lee, K.; Rivnay, J.; Yoon, M.-H. Influence of PEDOT:PSS crystallinity and composition on electrochemical transistor performance and long-term stability. *Nat. Commun.* **2018**, *9*, 3858.
(37) Kiefer, D.; Giovannitti, A.; Sun, H.; Biskup, T.; Hofmann, A.; Koopmans, M.; Cendra, C.; Weber, S.; Anton Koster, L. J.; Olsson, E.; Rivnay, J.; Fabiano, S.; McCulloch, I.; Müller, C. Enhanced n-Doping Efficiency of a Naphthalenediimide-Based Copolymer through Polar Side Chains for Organic Thermoelectrics. *ACS Energy Lett.* **2018**, *3*, 278−285.
(38) Liu, J.; Qiu, L.; Alessandri, R.; Qiu, X.; Portale, G.; Dong, J.; Talsma, W.; Ye, G.; Sengrian, A. A.; Souza, P. C. T.; Loi, M. A.; Chiechi, R. C.; Marrink, S. J.; Hummelen, J. C.; Koster, L. J. A.

https://dx.doi.org/10.1021/acsami.0c16254
ACS Appl. Mater. Interfaces 2020, 12, 53003−53011

Enhancing Molecular n-Type Doping of Donor-Acceptor Copolymers by Tailoring Side Chains. *Adv. Mater.* **2018**, *30*, 1704630.
(39) Hofmann, A. I.; Kroon, R.; Yu, L.; Müller, C. Highly stable doping of a polar polythiophene through co-processing with sulfonic acids and bistriflimide. *J. Mater. Chem. C* **2018**, *6*, 6905−6910.
(40) Müller, C. On the Glass Transition of Polymer Semiconductors and Its Impact on Polymer Solar Cell Stability. *Chem. Mater.* **2015**, *27*, 2740−2754.
(41) Babel, A.; Jenekhe, S. A. High Electron Mobility in Ladder Polymer Field-Effect Transistors. *J. Am. Chem. Soc.* **2003**, *125*, 13656−13657.
(42) Wang, S.; Sun, H.; Ail, U.; Vagin, M.; Persson, P. O. Å.; Andreasen, J. W.; Thiel, W.; Berggren, M.; Crispin, X.; Fazzi, D.; Fabiano, S. Thermoelectric Properties of Solution-Processed n-Doped Ladder-Type Conducting Polymers. *Adv. Mater.* **2016**, *28*, 10764−10771.
(43) Sun, H.; Vagin, M.; Wang, S.; Crispin, X.; Forchheimer, R.; Berggren, M.; Fabiano, S. Complementary Logic Circuits Based on High-Performance n-Type Organic Electrochemical Transistors. *Adv. Mater.* **2018**, *30*, 1704916.
(44) Winberg, H. E.; Carnahan, J. E.; Coffman, D. D.; Brown, M. Tetraaminoethylenes. *J. Am. Chem. Soc.* **1965**, *87*, 2055−2056.
(45) Zeng, Y.; Zheng, W.; Guo, Y.; Han, G.; Yi, Y. Doping mechanisms of N-DMBI-H for organic thermoelectrics: hydrogen removal vs. hydride transfer. *J. Mater. Chem. A* **2020**, *8*, 8323−8328.
(46) Wilbourn, K.; Murray, R. W. The electrochemical doping reactions of the conducting ladder polymer benzimidazobenzophenanthroline (BBL). *Macromolecules* **1988**, *21*, 89−96.
(47) MacDonald, W. A. Engineered films for display technologies. *J. Mater. Chem.* **2004**, *14*, 4−10.
(48) Bin, Z.; Duan, L.; Qiu, Y. Air Stable Organic Salt As an n-Type Dopant for Efficient and Stable Organic Light-Emitting Diodes. *ACS Appl. Mater. Interfaces* **2015**, *7*, 6444−6450.
(49) Fazzi, D.; Fabiano, S.; Ruoko, T.-P.; Meerholz, K.; Negri, F. Polarons in π-conjugated ladder-type polymers: a broken symmetry density functional description. *J. Mater. Chem. C* **2019**, *7*, 12876−12885.
(50) Briseno, A. L.; Mannsfeld, S. C. B.; Shamberger, P. J.; Ohuchi, F. S.; Bao, Z.; Jenekhe, S. A.; Xia, Y. Self-Assembly, Molecular Packing, and Electron Transport in n-Type Polymer Semiconductor Nanobelts. *Chem. Mater.* **2008**, *20*, 4712−4719.
(51) Wei, P.; Oh, J. H.; Dong, G.; Bao, Z. Use of a 1H-Benzoimidazole Derivative as ann-Type Dopant and To Enable Air-Stable Solution-Processedn-Channel Organic Thin-Film Transistors. *J. Am. Chem. Soc.* **2010**, *132*, 8852−8853.
(52) Reenen, S. v.; Kemerink, M. Correcting for contact geometry in Seebeck coefficient measurements of thin film devices. *Org. Electron.* **2014**, *15*, 2250−2255.

https://dx.doi.org/10.1021/acsami.0c16254
ACS Appl. Mater. Interfaces 2020, 12, 53003−53011